2019 American Control Conference (ACC)
Philadelphia, PA, USA, July 10-12, 2019

Robust Control of Wave Energy Converters Using Spectral and Pseudospectral Methods: A Case Study*

Demián García-Violini[♣,♦] and John V. Ringwood[♣,♠]

***Abstract*— Although *Spectral* and *Pseudospectral* methods have been used in a wide range of optimal control applications, to date, most of the literature uses these methods in a non-robust sense without considering possible dynamic deviation (uncertainties) from the nominal model. This study applies a recent robust approach for spectral and pseudospectral methods to a wave energy converter, considering structured uncertainty in the dynamical system. The results show that the robust approach gives better worst-case performance than an equivalent non-robust approach. Additionally, when structured uncertainty is considered in the dynamical system, the results show that the absorbed energy, obtained with the robust approach, is always positive. Finally, the advantages of this new approach are commented.**

I. INTRODUCTION

Spectral and pseudospectral methods, have been widely reported in the bibliography in diverse optimal control applications such as boundary value and eigenvalue problems, and also objective function optimisation (maximisation or minimisation) ([1]). One reason for the popularity of these methods is the user-selectable trade-off between computational effort and solution precision. However, to date, robust approaches, which allow for the description of the system with dynamical uncertainty, are not available ([2]).

For a further discussion about spectral and pseudospectral methods, the reader is referred to [1] and [3].

For the growing area of wave energy converter (WEC) energy maximising control ([4]), spectral and pseudospectral methods have been demonstrated to be appealing. The features which make spectral and/or pseudospectral methods useful in that application are worth highlighting. Firstly, the oscillatory nature that governs the problem makes this approach interesting, since waves can be approximately described as a multi-periodic process. With the purpose of approximating the periodic nature of the problem, the use of spectral and pseudospectral methods, with *Fourier* and *Chebyshev-Fourier* basis functions has been shown in [1] and [5], respectively. On the other hand, the use of these methods in WEC control has a significant impact on the simplification of the convolution integral associated with the radiation force. Moreover, as shown in [1], the bulk of the computation involving the numerical computation of the convolution integral can be carried out off-line, thus significantly reducing the computational load when solving the nonlinear program. The final aspect that makes the WEC control problem amenable, using spectral or pseudospectral methods, is the transformation of the integral objective function that should be maximised.

Although spectral and pseudospectral methods have been widely used to address different applications with linear and nonlinear descriptions, most of the recent literature uses these methods in a non-robust sense, without considering possible dynamic deviation (uncertainties) from the nominal model ([2]). While adaptive control is one way to deal with possible uncertainties, adaptive approaches do not give guarantees of convergence as shown in [6]. Alternatively, nonlinear approaches can deal with nonlinear deviations from a linear model, though these approaches depend on a precise nonlinear description of the model.

Considering the lack of robustness analysis for spectral and pseudospectral methods in general optimisation control problems, [7] redefines the traditional approach for such methods, taking dynamical uncertainty into account[1]. In this new framework, the objective is to ensure the 'best worst-case performance' (best-WCP), which involves the determination of a control signal which minimises the performance degradation in the objective function, when the system under study has uncertainty in its description. This paper studies the application procedure of the robust control strategy developed in [7] to a cylindrical WEC, considering dynamical uncertainty in the model description. The results obtained with the robust approach ([7]) are compared to those obtained with an equivalent non-robust approach ([1]), assessing the robustness of each controller when the system dynamical model includes different uncertainty levels.

The remainder of this paper is organised as follows. Firstly, Sec. II recalls: (1) the basics of spectral and pseudospectral methods; (2) the physical equations for WEC; and (3) the derivation of the objective function. The optimisation problem, which will guarantee the best-WCP condition, is shown in Sec. III. In Sec. IV the robust approach is applied to a cylindrical WEC system, comparing the results against those obtained with the nominal approach. Finally, conclusions are given in Sec. V.

II. PRELIMINARIES

The purpose of this section is to state the basics ideas that will be used in the development of the robust method in

* This material is based upon works supported by Science Foundation Ireland under Grant no. 13/IA/1886.

♣ Centre for Ocean Energy Research, Maynooth University, Co. Kildare, Ireland.
♦ e-mail (corresponding author): demian.garciaviolini@mu.ie
♠ e-mail: john.ringwood@mu.ie

[1]The framework proposed in [7] is an intermediate step in a number of implementable feedforward control strategies such as, for example, receding horizon control-based strategies. The interested reader is referred to [5] for a description of the implementation of these control structures.

978-1-5386-7926-5/$31.00 ©2019 AACC

Sec. III. With this aim, general concepts around spectral and pseudospectral methods, the general WEC equations, and the objective function are introduced. Finally, the optimal results for the nominal case are shown. This section can be studied in greater depth, by following the development in [1].

A. Spectral and Pseudospectral Methods

Spectral and pseudospectral methods are based on a projection of the states and control variables into an n-dimensional vector space spanned by an orthogonal basis of real functions $\Phi = \{\phi_i\}_{i=1}^{N}$. Given a dynamical system $\dot{x}(t) = f(x(t), u(t))$, its states $x_i(t)$, $i \in \{1, \ldots, n\}$, and input $u(t)$ are typically approximated as:

$$x_i(t) \approx x_i^N(t) = \sum_{j=1}^{N} \phi_j(t) x_{ij} = \Phi(t)\hat{\mathbf{x}}_i \tag{1a}$$

$$u(t) \approx u^N(t) = \sum_{j=1}^{N} \phi_j(t) u_j = \Phi(t)\hat{\mathbf{u}} \tag{1b}$$

where $\Phi(t) = \begin{bmatrix}\phi_1(t) & \ldots & \phi_N(t)\end{bmatrix}$ is an orthogonal set of basis functions, $\hat{\mathbf{x}}_i = \begin{bmatrix}x_{i1} & \ldots & x_{iN}\end{bmatrix}^\intercal \in \mathbb{R}^N$ and $\hat{\mathbf{u}} = \begin{bmatrix}u_1 & \ldots & u_N\end{bmatrix}^\intercal \in \mathbb{R}^N$. The sets of coefficients $\{x_{ij}\}$ and $\{u_j\}$ are determined by forcing the projection of the residual functions over the set of test functions Ψ to be zero ([1]). When $\psi_j = \delta(t - t_j)$, i.e. translated Dirac-Delta functions, then the method is termed pseudospectral, and guarantees the interpolation at t_j. When the set of test functions is defined by a truncated generalized Fourier series, and $\{\phi_j\} = \{\psi_j\}$, the method is known as spectral. In general, a wide variety of test functions can be used for spectral and pseudospectral methods, depending on the suitability for particular applications.

B. WECs and Objective Function

Assuming that the fluid is inviscid and incompressible, and the flow is considered irrotational, WEC systems are commonly described by Cummins' equation ([8]):

$$(m_b + m_\infty)\ddot{x}_p(t) + \int_0^T k(t-\tau)\dot{x}_p(\tau)d\tau + \\ + \mathbf{S}x_p(t) = F_e(t) + u(t) \tag{2}$$

where $x_p(t)$, $\dot{x}_p(t) = v(t)$, and $\ddot{x}_p(t)$, represent the WEC position, velocity, and acceleration, respectively, m_b is the mass of the oscillating body, m_∞ the added mass at infinite frequency, and $\mathbf{S}$ a positive constant describing the hydrostatic stiffness, which is related to the buoyancy force. The radiation impulse response $k(t)$, in Eq. (2), is related to the radiation force, which is a damping force arising to the fact that device motion is affected by the surrouding fluid. Additionally, in Eq. (2), the excitation force $F_e(t)$ is produced by the action of the incoming waves (energy source), and $u(t)$ is the control force generated by the power take-off (PTO) system, which is commonly used to maximise the energy production. The interested reader is referred to [9] for an exhaustive analysis of WEC dynamics. Then, the total absorbed energy in the interval $[0\ T]$, can be calculated as the integral of the converted power

$$J = -\int_0^T v^\intercal(t)u(t)dt, \tag{3}$$

where $u(t)$ and $v(t)$ are defined in Eq. (2). Generally, the optimal problem in WEC control is to maximise the captured energy J, defined in Eq. (3) as the integral of the instantaneous power, in a device which is subject to an external excitation force $F_e(t)$ while it is controlled via a control force $u(t)$.

Due to the orthogonality of the basis functions ϕ_j, the application of spectral or pseudospectral approximations to the objective function J as in Eq. (1), results in:

$$J \approx J_N = \int_0^T \hat{\mathbf{u}}^\intercal \Phi^\intercal(t)\Phi(t)\hat{\mathbf{v}} = -\frac{T}{2}\hat{\mathbf{u}}^\intercal\hat{\mathbf{v}} \tag{4}$$

where $\hat{\mathbf{v}} = \begin{bmatrix}v_1 & v_2 & \ldots & v_N\end{bmatrix}^\intercal \in \mathbb{R}^N$ corresponds to the approximation of $v(t)$, which be can obtained by a linear combination of the vectors $\hat{\mathbf{x}}_i$ in Eq. (1a), and $\hat{\mathbf{u}} = \begin{bmatrix}u_1 & u_2 & \ldots & u_N\end{bmatrix}^\intercal$ is stated in Eq. (1b).

Given the set Φ of basis functions, suppose that

$$\dot{\Phi}(t) = \Phi(t)\mathbf{D}, \tag{5}$$

where $\mathbf{D} \in \mathbb{R}^{n\times n}$, holds. Then

$$\hat{\mathbf{v}} = \mathbf{G_o}\left(\hat{\mathbf{u}} + \hat{\mathbf{e}}\right), \tag{6}$$

where $\mathbf{G_o}$ represents the mapping between $\hat{\mathbf{u}} + \hat{\mathbf{e}}$, which is the approximation of the input $u_i(t) = u(t) + F_e(t)$, and $\hat{\mathbf{v}}$, which is the approximation of the output $v(t)$. Additionally, in Eq. (6), $\hat{\mathbf{e}} = \begin{bmatrix}e_1 & e_2 & \ldots & e_N\end{bmatrix}^\intercal \in \mathbb{R}^N$, where the set $\{e_i\}_{i=1}^N$ contains the coefficients of the excitation force $F_e(t)$ approximation on the basis $\Phi(t)$, i.e $F(t) \approx \Phi(t)\hat{\mathbf{e}}$. When the basis functions are chosen appropriately, $\mathbf{G_o}$ satisfies

$$\mathbf{G_o} = \bigoplus_{k=1}^{N/2} \begin{bmatrix}\mathcal{R}_k^o & \mathcal{I}_k^o \\ -\mathcal{I}_k^o & \mathcal{R}_k^o\end{bmatrix}, \tag{7}$$

with $\mathcal{R}_k^o$, $\mathcal{I}_k^o \in \mathbb{R}$, $\mathbf{G_o} \in \mathbb{R}^{N\times N}$ and the symbol $\bigoplus$ denotes the direct sum of n matrices, i.e. $\bigoplus_{i=1}^n A_i = \text{diag}\{A_1, A_2, \ldots, A_n\}$. Note that in Eq. (7), without loss of generality, the number of basis functions is taken to be even. It is important to note that, due to the 2×2 block diagonal nature of the representation $\mathbf{G_o}$, defined in Eq. (7), $\mathbf{G_o}$ can be depicted in the plane $\mathcal{R} \times \mathcal{I}$.

C. Nominal Optimal Solution

By substituting Eq. (6) into the approximate absorbed energy expression in Eq. (4), the following equality is obtained:

$$J_N = -\frac{T}{2}\hat{\mathbf{u}}^\intercal\mathbf{G_o}\left(\hat{\mathbf{u}} + \hat{\mathbf{e}}\right) \tag{8}$$

which is a quadratic function of the variable $\hat{\mathbf{u}}$. In essence, the state variables have been eliminated by substitution, and the optimisation is carried out over the control variable $\hat{\mathbf{u}}$ only. More importantly, the constrained optimisation problem, given by the objective function describing the

total absorbed energy J_N, and the linear equality constraints describing the system dynamics in Eq. (6), has been transformed into an unconstrained quadratic program. Additionally, since the radiation damping term in Eq. (2) is a dissipative process ([9]), the radiation resistance is positive, and all the diagonal elements of the matrix $\mathbf{G_o}$ are positive. The absorbed energy function, stated in Eq. (8), is therefore concave, which guarantees the existence of a global maximum for the objective function. The concavity of the objective function will be used as a feasibility condition.

Therefore, the optimal formulation is stated as

$$\hat{\mathbf{u}}_o^\star \leftarrow \max_{\forall \hat{\mathbf{u}}_o \in \mathbb{R}^N} \; J_N \tag{9}$$

where $\mathbf{u_o}^\star$, for the unconstrained quadratic problem, which maximises Eq. (4), is then:

$$\hat{\mathbf{u}}_o^\star = -\left(\mathbf{G_o} + \mathbf{G_o}^\intercal\right)^{-1} \mathbf{G_o} \hat{\mathbf{e}}. \tag{10}$$

Thus, the control force coefficient vector $\hat{\mathbf{u}}_o^\star$, for the nominal case, is obtained in terms of excitation force approximation, which is given by the vector $\hat{\mathbf{e}}$, as shown in Eq. (6). Using Eq. (10), the approximate optimal control force $u_o^\star(t)$ can be obtained, as stated in Eq. (1b). The interested reader is referred to [9] for more details about realistic implementation of WEC energy maximising controllers.

III. GENERIC SOLUTION FOUNDATIONS

To proceed with the robust approach description, it is necessary to have a precise characterisation of the system. This section can be followed in-depth in [7].

In a more realistic situation, when the real system $\mathbf{G}$ does not match the nominal one, a representation of the real system can be obtained by the addition of a bounded disturbance $\mathbf{\Delta} \in \mathbb{R}^{N\times N}$:

$$\mathbf{G} = \mathbf{G_o} + \mathbf{\Delta}, \tag{11}$$

where $\mathbf{\Delta}$ must be properly structured, depending on the selected basis functions, and takes the following form:

$$\mathbf{\Delta} = \bigoplus_{k=1}^{N/2} \begin{bmatrix} \delta_k^{\mathcal{R}} & \delta_k^{\mathcal{I}} \\ -\delta_k^{\mathcal{I}} & \delta_k^{\mathcal{R}} \end{bmatrix} \tag{12}$$

which allows for the redefinition of the objective function:

$$J_N = -\frac{T}{2} \hat{\mathbf{u}}^\intercal \mathbf{G} \left(\hat{\mathbf{u}} + \hat{\mathbf{e}}\right) \tag{13}$$

A. Robust Approach: Best *W*orst-*C*ase *P*erformance

Using the feasibility condition for the nominal case defined in Sec. II-C, and defining the best-WCP solution as the input that minimises the performance degradation when the system under study is affected by a bounded uncertainty set Δ, then the robust statement can be defined as

$$\hat{\mathbf{u}}_r^\star \leftarrow \max_{\hat{\mathbf{u}}\in\mathbb{R}^N} \min_{\Delta\in\mathcal{U}} \; J_N \tag{14}$$

where $\mathcal{U}$ represents the set of all possible uncertainties. The definition in Eq. (14) is a robust quadratic formulation and, more generally, can be rewritten into a minimax problem ([10]). Furthermore, the uncertainty set must be defined properly in order to preserve the concavity and feasibility of the problem, as will be shown in Sec. III-B. On the other hand, since the problem is stated in the standard form used by minimax solvers, the formulation is amenable to the inclusion of constraints.

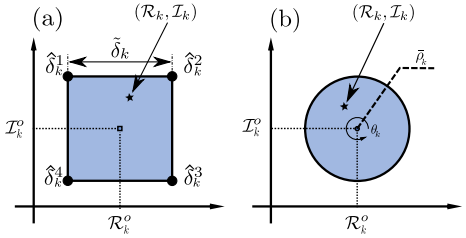

Fig. 1: Two different boundaries for the uncertainty set. **(a)** Convex polytopic set. **(b)** Convex and circular set.

Sections III-B, III-C, and III-D show the derivation of a solution for (14) in two different ways. Firstly, an analytical methodology is shown, for the case when the uncertainty is structured via circular and polytopic geometries. Then, a suboptimal numerical procedure, which can be applied to non-structured uncertainties, is shown.

B. Generic Solution Foundations

Here, a methodology to solve the problem stated in Eq. (14), is shown. The problem is solved using two different methodologies: one analytical and other numerical. For the analytical case, circular and polytopic uncertainty structures are addressed. In a discrete sense, by the use of a grid over the uncertainty set, for general uncertainty structures, a numerical, but suboptimal approach, is proposed.

General Comments: The general objective function, stated as in Eq. (13), can be rewritten as follows:

$$J_N = -\frac{T}{2}\left(\hat{\mathbf{u}}^\intercal \bigoplus_{k=1}^{N/2} \begin{bmatrix} e_k + u_k & e_{2k} + u_{2k} \\ e_{2k} + u_{2k} & -(e_k + u_k) \end{bmatrix} \bar{\delta} + f(\Upsilon)\right) \tag{15}$$

with $\bar{\delta} = \begin{bmatrix} \delta_1^{\mathcal{R}} & \delta_1^{\mathcal{I}} & \dots & \delta_{N/2}^{\mathcal{R}} & \delta_{N/2}^{\mathcal{I}} \end{bmatrix}^\intercal$ and $\Upsilon = [\hat{\mathbf{e}} \;\; \hat{\mathbf{u}} \;\; \mathcal{R}_k^o \;\; \mathcal{I}_k^o]$, which shows that J_N is affine in $\bar{\delta}$. Then, for a given $\hat{\mathbf{u}}$, $\hat{\mathbf{e}}$, and $\mathbf{G_o}$, the best-WCP solution is reached on the convex hull of the uncertainty set. Furthermore, when the uncertainty is structured as a convex polytope, if the optimal solution exists, it will be at one of the vertices of the polytope ([11]).

Figures 1(a) and 1(b) show two different examples of boundary schemes used for the development in [7], a convex polytope (specifically a square) and a circle, respectively. The set of all the possible locations of the real system is given by $\mathcal{P}_k$, where the points on and within the hull of the geometry are included. In particular, $(\mathcal{R}_k, \mathcal{I}_k)$ represents the location of the real system within the geometry, while $(\mathcal{R}_k^o, \mathcal{I}_k^o)$ is the location of the nominal system, as illustrated in Figures 1(a) and 1(b).

In the case of the convex polytope, as shown in Fig. 1(a), the geometry is defined by the set of vertices $\left\{ \hat{\delta}_k^1 \;\; \hat{\delta}_k^2 \;\; \dots \;\; \hat{\delta}_k^{p_k} \right\}$, where p_k defines the number of vertices of the polytope used in case k. Hence, each $\hat{\delta}_k^j = (\hat{\delta}_k^{\mathcal{R}^j}, \hat{\delta}_k^{\mathcal{I}^j})$ is defined such that the bounds of the real system

at the vertices are $\bar{\mathcal{R}}_k^j = \mathcal{R}_k^o + \hat{\delta}_k^{\mathcal{R}^j}$ and $\bar{\mathcal{I}}_k^j = \mathcal{I}_k^o + \hat{\delta}_k^{\mathcal{I}^j}$, with $j = 1, \ldots, p_k$.

The circular case, depicted in Fig. 1(b), can be defined in terms of a radius ρ_k and an angle θ_k

$$0 \leq \rho_k \leq \bar{\rho}_k \qquad 0 \leq \theta_k < 2\pi \tag{16}$$

Denoting $\mathrm{Re}\{\cdot\}$ and $\mathrm{Im}\{\cdot\}$ as the *real-part* and *imaginary-part* operators, respectively, then,

$$\delta_k^{\mathcal{R}} = \mathrm{Re}\left\{\rho_k \mathrm{e}^{\jmath\theta_k}\right\} \qquad \delta_k^{\mathcal{I}} = \mathrm{Im}\left\{\rho_k \mathrm{e}^{\jmath\theta_k}\right\}$$

which must be repeated for each k-block in Eq. (13). Then, for both cases (polytope and circle),

$$\mathcal{R}_k = \mathcal{R}_k^o + \delta_k^{\mathcal{R}} \qquad \mathcal{I}_k = \mathcal{I}_k^o + \delta_k^{\mathcal{I}} \tag{17}$$

where $\left(\delta_k^{\mathcal{R}}, \delta_k^{\mathcal{I}}\right)$ represents the deviation from the nominal model and $(\mathcal{R}_k, \mathcal{I}_k) \in \mathcal{P}_k$. On the other hand, Eq. (13) can be expressed as:

$$J_N = -\frac{T}{2}\sum_{k=1}^{N/2} \mathcal{R}_k(u_{2k-1}^2 + u_{2k}^2) + K\begin{bmatrix} u_{2k} \\ u_{2k-1} \end{bmatrix} \tag{18}$$

with $K = \begin{bmatrix} e_{2k}\mathcal{R}_k - e_{2k-1}\mathcal{I}_k & e_{2k}\mathcal{I}_k - e_{2k-1}\mathcal{R}_k \end{bmatrix}$. The expression in Eq. (18) shows that the problem concavity will be consistent (for both the nominal and real systems), with the sign of each $\mathcal{R}_k$. Thus,

$$\mathcal{R}_k = \mathcal{R}_k^o + \delta_k^{\mathcal{R}} > 0 \tag{19}$$

Eq. (19) explicitly shows the feasibility condition mentioned in Sec. II-C, for the nominal ($\delta_k^{\mathcal{R}} = 0$) and robust ($\delta_k^{\mathcal{R}} \neq 0$) cases. If the expression in Eq. (19) is greater than zero, then concavity is guaranteed, and thus the maximisation problem stated in Eq. (8), as a quadratic programming problem, has a feasible formulation and an optimal solution.

Finally, if the optimal solution can be expressed as:

$$\hat{\mathbf{u}}^\star = \bigoplus_{k=1}^{N/2} -\frac{1}{2}\begin{bmatrix} 1 & \frac{\mathcal{I}_k}{\mathcal{R}_k} \\ -\frac{\mathcal{I}_k}{\mathcal{R}_k} & 1 \end{bmatrix}\hat{\mathbf{e}} \Leftrightarrow \left.\frac{\partial J_N}{\partial \hat{\mathbf{u}}}\right|_{\hat{\mathbf{u}}=\hat{\mathbf{u}}^\star} = 0 \tag{20}$$

then, by substituting $\hat{\mathbf{u}}^\star$ from Eq. (20) into Eq. (13),

$$J_N^\star = \frac{T}{8}\sum_{k=1}^{N/2} \frac{\left(\mathcal{R}_k^2 + \mathcal{I}_k^2\right)\left(e_{2k-1}^2 + e_{2k}^2\right)}{\mathcal{R}_k} \tag{21}$$

In Sections III-C and III-D two solution methodologies for the best-WCP, are shown. The first, in Sec. III-C, based on an analytic approach, is limited to circular and polytopic convex boundaries. In Sec. III-D, the scope of the problem is extended, via a numerical formulation, to consider uncertainty sets of arbitrary shape.

C. Analytical Solution Approach

1) Circular Boundary: Due to the fact that the solution will be reached on the hull of the circle ($\rho_k = \bar{\rho}_k$), $\mathcal{R}_k$ and $\mathcal{I}_k$ can be replaced by:

$$\mathcal{R}_k = \mathcal{R}_k^o + \delta_k^{\mathcal{R}} = \mathcal{R}_k^o + \bar{\rho}_k \cos\theta_k \tag{22a}$$

$$\mathcal{I}_k = \mathcal{I}_k^o + \delta_k^{\mathcal{I}} = \mathcal{I}_k^o + \bar{\rho}_k \sin\theta_k \tag{22b}$$

Replacing Eq. (22a) and (22b) in Eq. (21), $J_N^\star(\theta_1, \ldots, \theta_{\frac{N}{2}})$ is defined. Then,

$$\hat{\mathbf{u}}_r^\star = \bigoplus_{j=1}^{N/2} -\frac{1}{2}\begin{bmatrix} 1 & \mathcal{B}_k^\star \\ -\mathcal{B}_k^\star & 1 \end{bmatrix}, \quad \text{where} \quad \mathcal{B}_k^\star = \frac{\mathcal{I}_k^o + \bar{\rho}_k \sin\theta_k{}^\star}{\mathcal{R}_k^o + \bar{\rho}_k \cos\theta_k{}^\star} \tag{23}$$

To obtain the best-WCP, the minimum value of $J_N^\star(\theta_1, \ldots, \theta_{\frac{N}{2}})$ is studied. Then

$$\left.\frac{\partial J_N^\star}{\partial \theta_k}\right|_{\theta_k=\theta_k^\star} = 0 \Rightarrow \theta_k^\star = \frac{c_k^3}{\sqrt{{c_k^1}^2 + {c_k^2}^2}} - \arctan\frac{c_k^1}{c_k^2} \tag{24}$$

with

$$c_k^1 = 2\mathcal{I}_k^o\mathcal{R}_k^o \quad c_k^2 = \bar{\rho}_k^2 + \mathcal{I}_k^o - {\mathcal{R}_k^o}^2 \quad c_k^3 = -2\bar{\rho}_k\mathcal{I}_k^o \tag{25}$$

which gives the location for θ_k where J_N reaches the minimum over $\mathcal{U}$.

Replacing Eq. (24) in (23), the input $\hat{\mathbf{u}}_r^\star$ that guarantees the best-WCP is obtained. Finally, the best-WCP is given by:

$$J_N^{WCP} = J_N^\star(\theta_1^\star, \ldots, \theta_{\frac{N}{2}}^\star)$$

2) Polytopic Boundary: For the polytopic boundary, using the fact, that if the optimal solution exists it will be on a vertex of the polytope. Then, for each $\mathcal{P}_k$ defined in Sec. III-B, using Eq. (21)

$$(\mathcal{R}_k^{j^\star}, \mathcal{I}_k^{j^\star}) \leftarrow j_k^\star \leftarrow \min_{j_k=1,\ldots,p_k} \left.J_N^\star\right|_{\mathcal{R}_k=\bar{\mathcal{R}}_k^j,\ \mathcal{I}_k=\bar{\mathcal{I}}_k^j} \tag{26}$$

for $j_k = 1, \ldots, p_k$ and $k = 1, \ldots, N/2$. Defining the vertex for each k where the WCP is reached, Eq. (20) is used for the computation of $\hat{\mathbf{u}}_r^\star$. Then,

$$J_N^{WCP} = J_N^\star(\mathcal{R}_k^{j^\star}, \mathcal{I}_k^{j^\star}, \ldots, \mathcal{R}_{\frac{N}{2}}^{j^\star}, \mathcal{I}_{\frac{N}{2}}^{j^\star})$$

D. Numerical Approach and Custom Bounding

In order to pose the problem in a standard form, Eq. (14) is rewritten into a minimax framework:

$$\hat{\mathbf{u}}_r^\star \leftarrow \max_{\hat{\mathbf{u}}\in\mathbb{R}^N}\min_{\Delta\in\mathcal{U}} J_N = \min_{\hat{\mathbf{u}}\in\mathbb{R}^N}\max_{\Delta\in\mathcal{U}} -J_N \tag{27}$$

To proceed with the numerical approach for the solution, the uncertainty space is discretised (mesh). Different possible uncertainty sets, and their meshing in the plane defined by $\mathcal{R}$ and $\mathcal{I}$, can be chosen. To define the mesh, a detailed procedure is provided in [7] for four different sets: (1) non-polytopic convex, (2) polytopic convex, (3) non-convex polytopic, and (4) arbitrary points.

Once the discretisation is carried out, the problem is restated in terms of the discretised grid:

$$\min_{\hat{\mathbf{u}}\in\mathbb{R}^N}\max_{\Delta_i\in\mathcal{U}} \frac{T}{2}\hat{\mathbf{u}}^\intercal\mathbf{G}_i(\hat{\mathbf{u}} + \hat{\mathbf{e}}) \tag{28}$$

with $\mathbf{G}_i = \mathbf{G_o} + \mathbf{\Delta}_i$ where $\mathbf{\Delta}_i$ is the perturbation associated at each i-point selected for the grid.

Following these specifications, the problem is formulated in the standard minimax form for the use with numerical optimisation solvers. Even though constraints can be straightforwardly included when minimax problem solvers are used, the analytical study of the constrained case is not within the scope of this study.

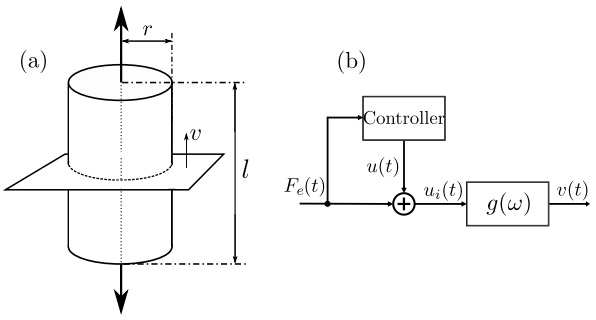

Fig. 2: **(a)** Physical model of the cylindrical WEC. **(b)** Cylindrical WEC and controller system block scheme.

IV. APPLICATION EXAMPLE

Using the results for the circular case shown in Sec. III, an application example, based on a cylindrical WEC model as depicted in Fig. 2(a), is shown here. For further details about WEC applications and definitions, the reader is referred to [9]. The radius r, the length l, and the mass m_b of the oscillating device are 4 m, 20 m, and 514 tons, respectively. The input and output to the nominal system $g_o(\omega)$ are the input force $u_i(t) = F_e(t)+u(t)$ and the device velocity $v(t)$, respectively, both defined for the vertical motion. In Fig. 2(b) a block diagram of the application example is illustrated, showing the input $u_i(t)$, the output $v(t)$, and the controller block.

The data for the nominal model $g_o(\omega)$ are generated using the boundary element methods-based environment NEMOH [12], obtaining the model frequency response $g_o(\omega)$, represented in Fig. 3.

For simplicity in the results illustration, this study is made assuming $N = 2$ ($\hat{\mathbf{u}}_o^\star$, $\hat{\mathbf{u}}_r^\star$, $\hat{\mathbf{e}} \in \mathbb{R}^2$ and $\mathbf{G}$, $\mathbf{G}_o \in \mathbb{R}^{2\times 2}$) and using the Fourier basis functions:

$$\mathbf{\Phi}(t) = \begin{bmatrix}\cos(\omega t) & \sin(\omega t)\end{bmatrix}. \tag{29}$$

In order to highlight the impact of the uncertainties included in the dynamical system $g_0(\omega)$, this study assumes perfect knowledge of the excitation force, and the vector $\hat{\mathbf{e}}$ is defined to be constant for the complete frequency range,

$$\hat{\mathbf{e}} = \alpha \begin{bmatrix}1 & 1\end{bmatrix}^\intercal, \ \forall\, \omega \text{ in Eq. (29) and constant } \alpha \in \mathbb{R}. \tag{30}$$

In a more realistic representation, $\hat{\mathbf{e}}$ should vary with frequency, as shown in [7]. However, with the simplification considered in Eq. (30), the variation of the resulting WEC performance only depends on the system (nominal or not) definition. In Eq. (30), an illustrative value $\alpha = 100$ has been chosen to simplify the visualisation of the resulting WEC performance.

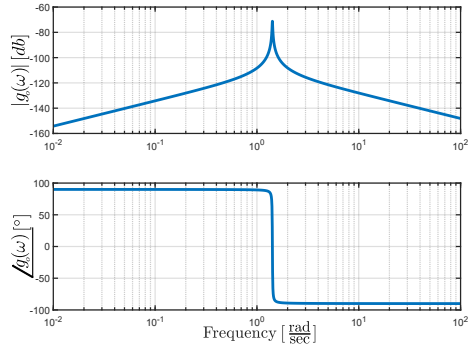

Fig. 3: Nominal system $g_o(\omega)$ frequency response.

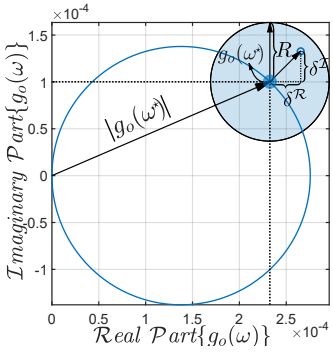

Fig. 4: Nyquist plot of $g_o(\omega)$ showing the circular boundary when $\omega = 1.412\,\frac{\text{rad}}{\text{sec}}$, assuming $R = 25\%$.

For each individual frequency, within the range $\omega^\star \in [0,\ 10]\ \frac{\text{rad}}{\text{sec}}$, the robust and nominal solutions are computed. A circular uncertainty boundary set, centred on $g_o(\omega^\star)$, is defined for each $\omega^\star$, using as maximum radius $\bar{\rho}$ (see Eq. (16)) as a percentage of the nominal system magnitude $|g_o(\omega^\star)|$; e.g. if the uncertainty level is R =25% then $\bar{\rho} = 0.25|g_o(\omega^\star)|$. In Fig. 4 the Nyquist plot for the nominal system $g_0(\omega)$ is represented with a solid blue line. Additionally, for the case $\omega^\star = 1.412\,\frac{\text{rad}}{\text{sec}}$, Fig 4 shows: (1) the nominal system magnitude $|g_o(\omega^\star)|$, illustrated with the long solid arrow; (2) the displacement effect of $\left(\delta^{\mathcal{R}},\ \delta^{\mathcal{I}}\right)$ from the nominal system $g_o(\omega^\star)$, depicted by the blue solid marker, to any other position inside the boundary, illustrated with the empty circle marker; and (3) the uncertainty level $R = 25\%$. Finally, the integration time, for each different frequency case, is defined as $T^\star = 2\pi/\omega^\star$.

A. Results

The main aim of this study is to assess the impact of the size of the boundaries, i.e. the conservativeness of the boundary, on the resulting performance, for the cylindrical WEC model, using the robust approach. Furthermore, a comparison with the resulting WCP, when the nominal solution is applied to the system with uncertainty, is made.

Considering circular boundaries, three different uncertainty levels, R =10%, 25% and 50%, are studied, for which the robust input $\hat{\mathbf{u}}_r^\star$, is calculated. When the nominal system $g_o(\omega)$ is considered, the nominal input $\hat{\mathbf{u}}_o^\star$ is obtained.

The resulting WCP, when each input $\hat{\mathbf{u}}_r^\star$, computed for each respective boundary, is applied to the complete set of models, is shown in Fig. 5. The performance achieved with the nominal control input $\hat{u}_o^\star$ is also shown for reference. Additionally, in Fig. 5: (1) the nominal performance (NP), obtained when the nominal model is considered without uncertainty, is plotted using the dotted line; (2) the WCP, obtained by applying $\hat{\mathbf{u}}_o^\star$ to the complete family set, is plotted using the dashed line; and (3) the WCP, obtained by applying $\hat{\mathbf{u}}_r^\star$ to the complete family set, is plotted using the solid line. The different uncertainty levels, depicted with the grey scale, are shown on the right-hand side in Fig. 5. Although the

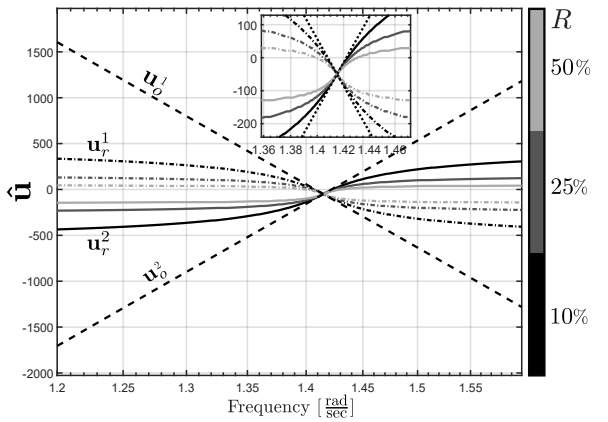

Fig. 5: Comparison of the WCP obtained with the robust and nominal approaches. The different uncertainty levels are depicted with the grey scale. The results for $\hat{\mathbf{u}}_r^\star$ and $\hat{\mathbf{u}}_o^\star$ are plotted with solid and dashed lines, respectively. The dotted line represents the result for the nominal performance (NP) considering the system $g_o(\omega)$ without uncertainty.

analysis is made for the range $\omega \in [0,\ 10]\ \frac{\text{rad}}{\text{sec}}$, the most significant results are within $\omega \in [1.2,\ 1.6]\ \frac{\text{rad}}{\text{sec}}$, mainly around $\omega = 1.41\ \frac{\text{rad}}{\text{sec}}$ (where the nominal system has its resonance frequency), as shown in Fig. 5. The coordinate location for $\hat{\mathbf{u}}_o^\star$, and the different robust inputs $\hat{\mathbf{u}}_r^\star$, are shown in Fig. 6, where: (1) for the nominal input, $\hat{\mathbf{u}}_o^\star = \begin{bmatrix}\mathbf{u}_o^1 & \mathbf{u}_o^2\end{bmatrix}^\intercal$, the first and second coordinate, labelled with $\mathbf{u}_o^1$ and $\mathbf{u}_o^2$ respectively, are depicted with the dashed line; (2) for the robust input,$\hat{\mathbf{u}}_r^\star = \begin{bmatrix}\mathbf{u}_r^1 & \mathbf{u}_r^2\end{bmatrix}^\intercal$, using the same grey scale code as in Fig. 5, the first and second coordinate, labelled with $\mathbf{u}_r^1$ and $\mathbf{u}_r^2$ respectively, are illustrated with the dash-dot and solid lines, respectively.

B. Results Analysis

Comparing the results obtained, using different circular uncertainty set cases, the impact of the size of the boundaries is highlighted. The larger the boundary is, the more conservative the approach, and the lower the consequent performance. Furthermore, Fig. 6 shows that the robust approach never results in the *consumption* of power, while the nominal controller results in negative energy, for some

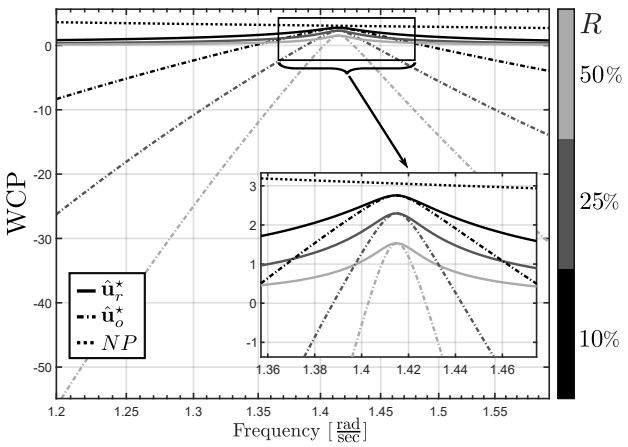

Fig. 6: Coordinate location for each $\hat{\mathbf{u}}_r^\star = \begin{bmatrix}\mathbf{u}_r^1 & \mathbf{u}_r^2\end{bmatrix}^\intercal$ and $\hat{\mathbf{u}}_o^\star = \begin{bmatrix}\mathbf{u}_o^1 & \mathbf{u}_o^2\end{bmatrix}^\intercal$. With the dashed line $\mathbf{u}_o^1$ and $\mathbf{u}_o^2$, are referred. The dash-dot and solid lines show the first and second coordinates of $\hat{\mathbf{u}}_r^\star$, respectively. The uncertainty level is indicated with the grey scale.

subset of ω. In addition, when the nominal approach is applied to the complete family of models, the larger the boundary is, the narrower is the band with positive energy consumption. In Fig. 6, at the system resonance frequency, both robust and non-robust approaches obtain the same worst-case performance, for each particular R. Finally, the performance obtained at the system resonance frequency is maximal over ω for each R, as shown in Fig. 6.

V. CONCLUSION

This study shows the application procedure, to a cylindrical WEC, of a new robust framework for computing and solving spectral and pseudospectral control problems in energy maximising problems with uncertainty. The results show how the robust approach ensures that the resulting absorbed energy will never be negative, guaranteeing positive generated energy. In this sense, this study shows how a correct uncertainty bound can significantly improve the results, exposing the existing trade-off between the conservativeness and the worst-case performance. In all cases, the nominal controller shows significant performance degradation for the nominal case compared to the robust approach. Finally, the robust approach provides convergence guarantees to the best-WCP, ensuring better performance for any model within the uncertainty bound. study.

ACKNOWLEDGMENT

This material is based upon works supported by Science Foundation Ireland under Grant no. 13/IA/1886. Thanks to Nicolás Faedo for the discussion during this study.

REFERENCES

[1] G. Bacelli and J. V. Ringwood, "Numerical optimal control of wave energy converters," *IEEE Transactions on Sustainable Energy*, vol. 6, no. 2, pp. 294–302, 2015.

[2] N. Faedo, S. Olaya, and J. V. Ringwood, "Optimal control, MPC and MPC-like algorithms for wave energy systems: An overview," *IFAC Journal of Systems and Control*, vol. 1, pp. 37–56, 2017.

[3] B. Fornberg, *A Practical Guide to Pseudospectral Methods*. Cambridge University Press, 1996.

[4] J. V. Ringwood, G. Bacelli, and F. Fusco, "Control, forecasting and optimisation for wave energy conversion," *IFAC Proceedings Volumes*, vol. 47, no. 3, pp. 7678–7689, 2014.

[5] R. Genest and J. V. Ringwood, "Receding horizon pseudospectral control for energy maximization with application to wave energy devices," *IEEE Transactions on Control Systems Technology*, vol. 25, no. 1, pp. 29–38, 2017.

[6] R. Genest, J. Davidson, and J. V. Ringwood, "Adaptive control of a wave energy converter," *IEEE Transactions on Sustainable Energy*, vol. 9, no. 4, pp. 1588–1595, 2018.

[7] D. Garcia-Violini and J. V. Ringwood, "Energy maximising robust control for spectral and pseudospectral methods with application to wave energy systems," *International Journal of Control*, 2018, under revision.

[8] W. E. Cummins, "The impulse response function and ship motions," *Schiffstechnik*, vol. 47, pp. 101–109, 1962.

[9] J. Falnes, *Ocean waves and oscillating systems: linear interactions including wave-energy extraction*. Cambridge University Press, 2002.

[10] S. Verdu and H. Poor, "On minimax robustness: A general approach and applications," *IEEE Transactions on Information Theory*, vol. 30, no. 2, pp. 328–340, 1984.

[11] S. Boyd and L. Vandenberghe, *Convex optimization*. Cambridge University Press, 2004.

[12] LHEEA, NEMOH-Presentation, "Laboratoire de Recherche en Hydrodynamique Énergetique et Environnement Atmospherique," https://goo.gl/yX8nFu, 2017, [Online accessed 11-Mar-2019].